Complex Flow Patterns in the Scheldt Estuary: Field Measurements and Validation of a Hydrodynamic Model

Y. Plancke[1]; J. Stark[2]; D. Meire[3]; and M. Schrijver[4]

Abstract: The morphology of the Scheldt estuary creates challenges for its different functions. Large shoals and adjacent channels with sharp bends result in challenging conditions for navigation. In order to provide estuarine managers with adequate answers, different research tools are necessary: numerical models, physical scale models, monitoring, and system understanding and expertise. This paper describes the validation of two numerical models, focusing on the Hansweert area, which is characterized by complex flow fields and important dredging works. In 2016, velocity measurements were executed over two spring-neap cycles using Acoustic Doppler Profiler devices. These velocity measurements are used for additional validation of two existing numerical models, describing the entire Scheldt estuary. Both models have shown good performance in large-scale tidal hydrodynamics, but uncertainty increases for local flow patterns, especially in shallow and intertidal areas. Adapting the local friction field improved significantly the representation of the measured complex flow patterns (e.g., large eddies) in the study area without impacting the overall model performance. This model allows both the improvement of our system understanding, e.g., formation of the large eddy, as well as the generation of flow patterns that are used in a ship simulator, where river pilots train to prepare for the challenging flow conditions in the field. **DOI: [10.1061/(ASCE)HY.1943-7900.0001737](https://doi.org/10.1061/(ASCE)HY.1943-7900.0001737).** *This work is made available under the terms of the Creative Commons Attribution 4.0 International license, https://creativecommons.org/licenses/by/4.0/.*

Introduction

Between the Flemish-Dutch authorities three main functions have been defined for the Scheldt estuary: port accessibility, safety against flooding, and ecology (Rijkswaterstaat Directie Zeeland and Ministry of the Flemish Government 2001). All of these functions are strongly affected by changes in morphology because the interplay between tides and estuarine morphology determines the tidal flow characteristics and hence sediment transports and sediment concentrations in estuaries (e.g., Townend and Pethick 2002; Wang et al. 1999). Consequently, morphological management of estuaries directly influences estuarine functioning. Port accessibility is, for example, guaranteed by fairway maintenance, whereas safety against flooding is affected by changes in tidal penetration due to land reclamation, sand mining, and fairway deepening (e.g., Smolders et al. 2015; Stark et al. 2017b). Furthermore, the ecological functioning of estuaries is influenced by morphological developments through subsequent changes in flow dynamics and sediment concentrations (e.g., van Maren and van Kessel 2016; Meire et al. 2005; Mitchell 2013; Winterwerp et al. 2013) and by

changes in intertidal habitats within the estuarine morphology and geometry (e.g., Cox et al. 2006; van der Wal et al. 2011). Several strategies can be applied for the morphological management of estuaries, including managed realignment or de-embankments (e.g., French 2006; Rupp-Armstrong and Nicholls 2007; Temmerman and Kirwan 2015), regular dredging and disposal strategies, or re-allocation of sediments to enhance tidal flat formation (e.g., Plancke et al. 2015; De Vriend et al. 2011).

The complex morphology of the Scheldt estuary creates challenging conditions for navigation. This is demonstrated by the grounding of the Fowairet, a 276.5-m long container vessel, in 2005. The Fowairet stranded on the shallow plateau between the sill of Hansweert and the Ossenisse shoal as a result of transient dangerous flow conditions. Extensive data analysis and numerical modeling allowed the Dutch government to set up a warning system for eddy-induced cross-currents. The occurrence and strength of cross-currents in the study area was found to be related to the high water level and maximum rising speed and a criterium *cr* for the occurrence of hazardous cross-currents was defined (Decrop et al. 2010):

$$cr = (1 + k_a(HWL - k_b))\left(\frac{\partial h}{\partial t}\right) \geq 4 \text{ cm/min} \qquad (1)$$

where *HWL* represents the high water level at Hansweert; $dhdt^{-1}$ = maximum rising speed during flood at Hansweert; and calibration parameters k_a and k_b are set to 1.0 and 0.55 [i.e., in case water levels are expressed in m (Normaal Amsterdams Peil, i.e. Dutch ordnance level (NAP)], respectively.

To provide estuarine managers with adequate answers, different tools are available and should be used at the same time: numerical models, physical scale models, monitoring, and system understanding and expertise (Peters et al. 2006). Where field measurements provide basic information on the system functioning, they are limited in spatial and/or temporal resolution. Therefore combining measurements with numerical and physical scale models is crucial in providing answers and optimizing estuarine management. The final goal of our study is the numerical model that allows the

---

[1]Flanders Hydraulics Research, Berchemlei 115, 2140 Antwerp, Belgium; Antwerp Port Authority, Zaha Hadidplein 1, 2030 Antwerp, Belgium; Guest Lecturer, Faculty of Applied Engineering, Antwerp Univ., Groenenborgerlaan 171, 2020 Antwerp, Belgium (corresponding author). ORCID: https://orcid.org/0000-0002-4303-082X. Email: yves.plancke@mow.vlaanderen.be

[2]Flanders Hydraulics Research, Berchemlei 115, 2140 Antwerp, Belgium. ORCID: https://orcid.org/0000-0002-5874-1704. Email: jeroen.stark@mow.vlaanderen.be

[3]Flanders Hydraulics Research, Berchemlei 115, 2140 Antwerp, Belgium. Email: dieter.meire@mow.vlaanderen.be

[4]Rijkswaterstaat Zee en Delta, Poelendaelesingel 18, 4335 JA Middelburg, Netherlands. Email: marco.schrijver@rws.nl

evaluation of the morphological effects of different management scenarios. However, the first step is to validate the present models for the hydrodynamics, using the interplay between field measurements and numerical models to improve insight in the complex flow patterns in the Scheldt estuary.
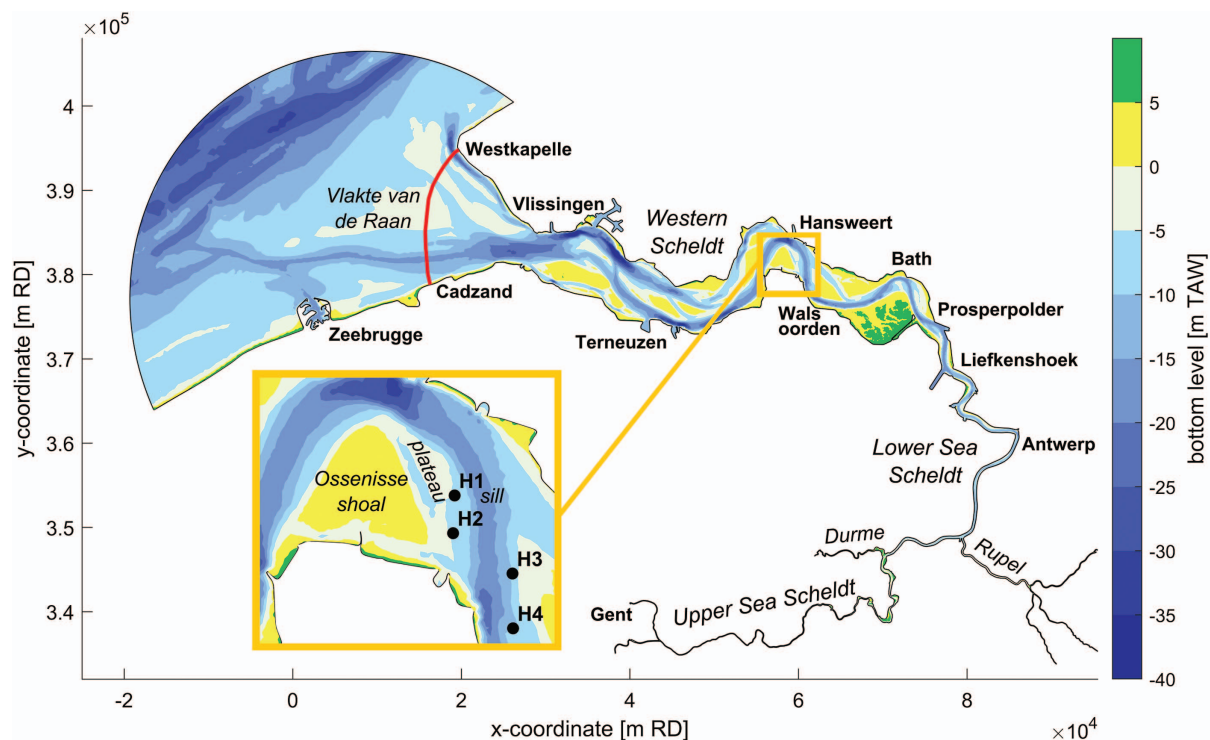
Scheldt Estuary

The Scheldt estuary is a 180-km-long macrotidal estuary in Belgium and SW Netherlands (Fig. 1). A shallow mouth, the Vlakte van de Raan (KM -20 to KM 0), connects the estuary with the North Sea and has several deeper channels (Elias et al. 2017). The Western Scheldt (KM 0 to KM 60) consists of a multiple channel system, with ebb and flood channels divided by intertidal sandbars. Further up-estuary, near the Dutch-Belgian border at Prosperpolder, the morphological system changes into a single channel system, the Lower and Upper Sea Scheldt (KM 60 to KM 160). Tributaries and side-branches include the Durme and Rupel rivers. The estuary is characterized by macrotidal semidiurnal tides, creating ebb and flood currents that carry both cohesive (mud) and noncohesive (sand) sediment loads (Baeyens et al. 1998). While cohesive sediment transport is most important in the up-estuarine part (Lower and Upper Sea Scheldt), sediment transport in the Western Scheldt is dominated by sand transport. To guarantee the accessibility towards the port of Antwerp, Europe's second largest port, maintenance dredging works have to be performed almost continuously. Specific temporal valid licenses have to be granted to execute the necessary dredging works, which, since the last enlargement of the navigation channel in 2010 (De Wit et al. 2007), vary between 10 and 15 Mm^3 annually.

The Belgian-Dutch research program, "Agenda for the Future," addresses system management challenges for the Scheldt estuary in the near future (e.g., tidal amplification, risk of regime shift towards a hyperturbid system, sediment management, improvement of ecological value). Furthermore, within the MONEOS monitoring program (Plancke et al. 2012), continuous water level measurements are performed at more than 20 locations along the estuary, as well as measurements of both flow velocities and physicochemical parameters at different point locations. Besides these continuous measurements, annual 13-h flow and discharge measurements across several transects in the estuary are done as well as annual topo-bathymetric sounding using single beam and multibeam echo soundings and LIDAR. On top of that, additional measurements are performed at specific areas of interest (e.g., sills and intertidal areas) to improve system understanding and to collect datasets for model validation. For example, velocity measurements are performed to validate the numerical models that are used on the one hand to derive flow characteristics (e.g., peak velocity, duration that flow velocity exceeds a certain threshold) for the classification of distinct ecological regions or ecotopes (van der Wal et al. 2017) within the scope of the NATURA 2000 European Directives. Furthermore, flow fields from numerical models are also used as basic information in ship simulators, where the feasibility is investigated of new generation container vessels using the navigation channel (e.g., Eloot and Verwilligen 2010).

Study Site

For this study, the area of interest concerns the sill of Hansweert and adjacent tidal flats and channels (Fig. 1). The present-day tidal range at Hansweert varies between 3.70 and 5.05 m for neap and spring tide respectively, resulting in strong tidal ebb and flood currents (up to 2 m/s). Near Hansweert, the navigational channel makes a sharp bend of almost 180°, causing strong secondary flows. At the inner bend of the navigation channel, the 4-km^2 intertidal flat of Ossenisse is located. Between the eastern edge of the Ossenisse sandflat and the sill of Hansweert in the navigation channel, lies a shallow subtidal area (plateau) of approximately 2 km^2 with a bed level at about −6 m TAW (i.e., TAW is the Belgian ordnance level, about 2.33 m below mean sea level), where the velocity

Fig. 1. (Color) Map of the Scheldt estuary, showing the Telemac (black) and Delft3D (red) model boundaries, main tidal stations, and the measurement locations near sill of Hansweert (gold).

Table 1. Measurement locations and periods

Parameter	Location			
	H1	H2	H3	H4
Measured interval	28/04/2016–26/05/2016	28/04/2016–10/05/2016	28/04/2016–03/05/2016	28/04/2016–11/05/2016
Duration (days)	27.5	11.5	4.9	13.2
Northing (m RD)	381,685	380,828	379,912	378,667
Easting (m RD)	60,130	60,095	61,444	61,457
Bottom level (m TAW)	−4.3	−5.9	−6.5	−9.9

measurements that are presented in this study were performed. The adjacent navigation channel has a depth of −15.2 m TAW. Annual maintenance dredging volumes are high at the sill of Hansweert (i.e., approximately 2–3 $Mm^3 y^{-1}$ from 2010 onwards according to Vos et al. 2017), while flow patterns are known to be complex due to the formation of large scale (i.e., ~2 km in diameter) eddies during spring tide high waters (Decrop et al. 2010). In particular, the tidal propagation over the Ossenisse sandflat during the flood phase of higher high waters is slow relative to the tidal propagation in the estuarine channel itself due to differences in bottom friction, resulting in a water level depression above the shoal. The subsequent water level gradients induce a return flow from the southeast towards the shallow plateau, which has an opposite direction than the regular flood tidal flow in the main channel. As the opposing flows enclose the water level depression above the shallow plateau, the flow field starts to curve due to water level gradients in the depression and an eddy is formed. The presence of these large scale eddies may cause cross-currents in the navigation channel, which can be dangerous for shipping traffic, e.g., the grounding of the Fowairet in 2005, and also more recently ships were confronted with the hazardous cross-currents at this location. Previous research suggested that the presence of the shallow plateau between the Ossenisse shoal and the Hansweert sill is of major importance for the development of a large horizontal eddy and associated cross-currents in the study area (Decrop et al. 2010). However, the extent of this shallow plateau increased since their study, while the Hansweert sill deepened due to capital dredging of the navigation channel (Plancke et al. 2015), potentially changing the presence and frequency of occurrence of these eddies and accompanying cross-currents.

Objectives

In this study, a velocity measurement campaign near the intensively dredged Hansweert sill in the main navigation channel of the Scheldt estuary is presented, as well as the validation of existing numerical models of the estuary based on these measurements. This study aims at: (1) identifying and improving insight into the present-day complex flow patterns around the sill of Hansweert using field measurements and numerical modeling; and (2) validating, comparing, and preferably also improving the model performance of two existing hydrodynamic models of the Scheldt estuary with regard to the representation of these flow patterns. Ultimately, beyond this first phase of the research, it is intended that these numerical models are used for sediment transport and morphological modeling in order to optimize dredging strategies.

Methods

Field Measurements

In 2016, a hydrodynamic measurement campaign was executed by Rijkswaterstaat near the sill of Hansweert in the Western Scheldt.

At four locations (Fig. 1 and Table 1), up-looking ADCPs (i.e., RD Instruments Workhorse Monitor 1,200 kHz) were deployed for two spring-neap cycles (April 28, 2016 until May 26, 2016). These devices provide directional velocity data which is processed with an output interval of 10 min. Two devices were placed on a shallow plateau between the sill of Hansweert and the Ossenisse shoal (i.e., H1 and H2) and two devices were placed at the other side of the sill near the Walsoorden shoal (i.e., H3 and H4), aiming at picturing the currents near the sill. During the measurement period, different ADCP's got buried under deposited sediment at different moments (Table 1), leading to incomplete time series over the full period. At location H3, the ADCP got buried after 5 days, causing the spring tide velocity data to be missing at that location.

Field measurements are analyzed focusing on water level (height of high water, gradients, rising velocity) and flow velocity parameters (maximum current, cross-current). Cross-currents are derived calculating the component perpendicular to the mean ebb and flood direction (as mean of absolute value of sinus of current direction) and are related to the formation of large eddies at the location H1 and H2.

Numerical Models

Two existing numerical models are compared in this study: a two-dimensional (2D) Delft3D model (Deltares 2016) and a three-dimensional (3D) Telemac-3D model (Hervouet 2007). Both models are extensively used to provide managers with answers within the scope of several projects in the Scheldt-estuary [e.g., sediment strategy (Ides et al. 2010) and Integrated plan of the Upper Sea Scheldt (Adams et al. 2016)]. A description of both models is given below. Model simulations are performed for the period of the field measurements after which modeled flow velocities are compared with the observations. Special focus is laid on the presence of velocity peaks related to the presence of large scale eddies (i.e., circular flow). Additionally, the modeled velocity fields in the study area around high water are analyzed for the spatial development and frequency of occurrence of large-scale eddies.

NeVla/Delft3D Model

The first numerical model used in this study is the existing NeVla 2D numerical model of the Scheldt estuary, which was set up in the SIMONA software package and later on exported to Delft3D (Maximova et al. 2014; Verheyen et al. 2013). The NeVla model grid comprises the Scheldt estuary from the mouth area between Cadzand and Westkapelle up until the upstream tributaries (Fig. 1). The model has a structured grid with a resolution in the zone of interest of 150 m (length) by 100 m (width). The implemented bathymetry consists of bathymetrical data of the year 2015 for the Western Scheldt, resulting form single beam echo soundings of equidistant (~100 m) spaced transects, interpolated onto a 20 × 20-m grid, and 5 × 5-m data from the year 2011 for the Sea Scheldt, generated from multibeam echo soundings with spatial resolution of 1 × 1 m. For the study area near the Hansweert sill, bathymetrical

data obtained during the measurement period (i.e., April 2016) is used. These local multibeam echo soundings (resolution 1×1 m) are more frequently (i.e., every 2–4 weeks) measured on the sills to ensure safe navigation and an extra multibeam echo sounding of a larger area near the Ossenisse sandbar was available within the scope of a disposal test. For this study, the downstream boundary of the model is forced with time series of observed water levels in the mouth area (i.e., data from the Westkapelle and Cadzand tidal stations from April 26, 2016 until May 31, 2016). According to findings from Vanlede et al. (2009) and Maximova et al. (2009), a +10 min phase shift is applied to the Cadzand water level series to correct for a 5,200-m difference between the model boundary and the actual Cadzand tidal station. The upstream boundaries are forced by yearly averaged discharges from Cornet and Mostaert (2010). Besides, discharge influences are expected to be negligible as the study area is situated in the downstream part of the estuary where the total river-induced flow of approximately 80 $\mathrm{m^3\,s^{-1}}$ only accounts for <1% of the tidally induced flow in the Western Scheldt (e.g., Stark et al. 2017a).

In Delft3D, the effect of turbulence is included by means of the spatially constant horizontal eddy viscosity parameter (ν_{hor}), which represents a scale for the lateral momentum diffusion. The horizontal eddy-viscosity is mostly associated with the contribution of horizontal turbulent motions and forcing that are not resolved (i.e., subgrid scale turbulence) either by the horizontal grid or a priori removed by solving the Reynolds-averaged shallow-water equations (Gerritsen et al. 2007). The optimal value of the eddy viscosity parameter is determined by the water depth and grid resolution, and it is suggested to use a value between 0.1 and 0.5 $\mathrm{m^2\,s^{-1}}$. In Decrop et al. (2009) it was shown that a higher value results in a damping of lateral velocity gradients and reduces the formation of the eddy. In accordance with previous modeling work by Decrop et al. (2010), this user-specified eddy viscosity is set at $\nu_{hor} = 0.1\ \mathrm{m^2\,s^{-1}}$ in the present study.

Initially, a uniform Manning bed roughness was applied (0.025 $\mathrm{m^{1/3}\,s^{-1}}$) in the subtidal channels, while a height-dependent value was chosen for intertidal areas, leading to a larger bed friction for vegetated salt marshes. These values were copied from the base model, which was calibrated on water levels throughout the estuary, as well as flow velocities on intertidal shoals (Ides and Plancke 2008). In this study, the bed roughness coefficients in the study area are changed to improve the representation of the measured flow velocities and the observed circular flow pattern in particular. More specifically, bottom friction coefficients are lowered on the shallow plateau and Ossenisse sandbar using the following algorithm [Fig. 2(b)]

$$z_b < -7.5\ \mathrm{m\,TAW} \quad n = 0.025\ \mathrm{m^{1/3}\,s^{-1}} \tag{2a}$$

$$-7.5\ \mathrm{m\,TAW} < z_b < -2.5\ \mathrm{m\,TAW} \quad n = 0.015 - 0.002 \cdot (z_b + 2.5)\ \mathrm{m^{1/3}\,s^{-1}} \tag{2b}$$

$$-2.5\ \mathrm{m\,TAW} < z_b < 2.5\ \mathrm{m\,TAW} \quad n = 0.015\ \mathrm{m^{1/3}\,s^{-1}} \tag{2c}$$

$$z_b > 2.5\ \mathrm{m\,TAW} \quad n = 0.015 + 0.01 \cdot (z_b - 2.5)\ \mathrm{m^{1/3}\,s^{-1}} \tag{2d}$$

where z_b represents the bottom elevation of each grid cell; and n = Manning coefficient. Physically, bed roughness can be related to grain size, e.g., Strickler (1923), on the one hand and bedforms, e.g., van Rijn (1984), on the other hand. However, due to large spatial variation in both grain size (100–300 μm) and bedforms (ranging from ripples to large dunes) within the study area, the theoretical approach was not applicable for our case. Alternatively, the final settings of the bottom friction coefficients were obtained in the calibration procedure, which aimed an optimal representation of the observed flow patterns. According to Chow (1959) these values are representative for dredged channels with no vegetation, which is applicable for our study area.

TELEMAC Model

A second numerical model was developed using the open source TELEMAC software. TELEMAC-3D is a finite-element hydrodynamic model with an unstructured grid that solves the Navier-Stokes equations in three dimensions. All parameter settings of the Telemac model used in this study are adopted from a previously
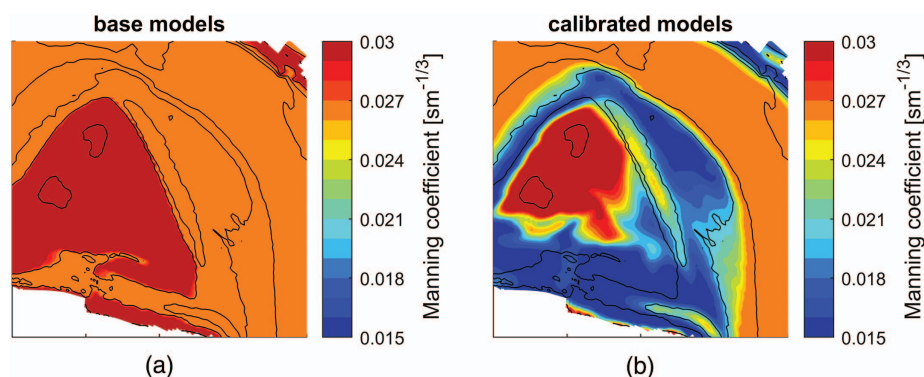
Fig. 2. (Color) Manning roughness fields in the study area for (a) the base models; and (b) calibrated NeVla model.

validated TELEMAC model of the Scheldt Estuary "Scaldis" and can be found in that model's validation report (Smolders et al. 2016). The only significant differences between the settings of the existing Scaldis model and of the TELEMAC model presented in this study are the extent and resolution of the model mesh. Comparison between the present model and the Scaldis model shows that the performance of both models is equally good in the Western Scheldt. The mesh resolution in the model domain varies from ~500 m in the offshore zone, ~150 m in the Western Scheldt, 50 m in the study area around Hansweert to 25–100 m in the Sea Scheldt and upstream tributaries. Hence, the TELEMAC model is locally refined and therefore has a finer resolution in the study area compared to the NeVla model (i.e., 50 m versus 100–150 m). The 3D model consists of five sigma-layers with the following distribution: $z*(1) = 0.0 \cdot h$ (i.e., bottom); $z*(2) = 0.12 \cdot h$; $z*(3) = 0.3 \cdot h$; $z*(4) = 0.6 \cdot h$; and $z*(5) = 1.0 \cdot h$ (i.e., surface), with $z(i)$ the elevation of each layer and h the water depth.

Based on the Scaldis model calibration (higher high waters betweenVanlede et al. 2015), a spatially varying (streamwise along the estuary) Manning bed roughness coefficient is initially applied in the TELEMAC model (i.e., ~0.022 m$^{1/3}$ s^{-1} in the Western Scheldt from where roughness coefficients generally stepwise decrease upstream). As for the NeVla model, the model is calibrated by altering the friction coefficients on the shoal of Ossenisse and on the shallow plateau between the Ossenisse shoal and the sill of Hansweert. More specifically, the bottom friction coefficient is lowered using the same procedure as described above for the NeVla model. Hence, bottom friction coefficients are lowered to a minimum value of 0.015 m$^{1/3}$ s^{-1} depending on the bottom elevation. However, the bottom friction coefficient in deeper subtidal parts and on the higher parts of the Ossenisse shoal is maximized to the surrounding value of 0.022 m$^{1/3}$ s^{-1}. Hence, the bottom roughness in the TELEMAC models slightly differs from the roughness fields that are shown in Fig. 2.

The settings for turbulence modeling are also adopted from the validated Scaldis model (Smolders et al. 2016). Horizontal turbulence is included by the Smagorinsky subgrid turbulence model, which is particularly recommended in the presence of a highly nonlinear flow (EDF R&D 2017; Hervouet 2007). The turbulent viscosity calculated with the Smagorinsky scheme (ν_t) is added to the user-specified laminar viscosity (i.e., set at $\nu_l = 10^{-2}$ m^2 s^{-1}) to calculate the total viscosity ($\nu_{tot} = \nu_t + \nu_l$). The bathymetrical data that is interpolated to the mesh is identical to the data used for the NeVla model, as is the upstream forcing. However, the downstream forcing differs between both models. While the NeVla model is cut off at the estuary mouth, the TELEMAC model used in this study extents further offshore into the North Sea (Fig. 1). This also implies that the offshore boundary conditions differ between the two models. In particular, the TELEMAC model is nested in a larger-scale continental shelf model, which is on its turn forced by harmonic components only and does not include surge effects, whereas the NeVla model was forced by measured water level series.

Scenarios

Numerical models allow better insight into physical processes by running specific scenarios. Over the past decades, the morphology and geometry of sandbars in the Scheldt estuary have changed significantly (de Vet et al. 2017). Accordingly, two scenarios were defined in order to evaluate the influence of the height of the Ossenisse sandbar on the development of the large eddies in the study area. These scenarios are only investigated with the NeVla model as this model is better able to reproduce the large eddy than the Scaldis model (see results section). In a first scenario, the intertidal part of the Ossenisse sandbar was lowered with 50% relative to mean low water level (i.e., multiply level above low water with factor 0.5)., which is an approximation of the situation in the past. In a second scenario, the intertidal part of the Ossenisse sandbar was heightened with 50% relative to the low water level (i.e., multiply level above low water with factor 1.5), which may not be a realistic future evolution, but allows to gain an insight in the role of the sandbar if part of it is not inundated or would become supratidal. Both scenarios are simulated with the roughness field of the calibrated NeVla model shown in Fig. 2(b).

Results

Field Measurements

Fig. 3 shows the measured flow velocities and directions during the measurement campaign from April 28, 2016 until May 13, 2016. At location H1 on the shallow plateau (Fig. 1), ebb velocities exceed flood velocities during lower tides, while flood velocities are higher during higher tides. During spring tide, flood velocities at location H1 are almost as high as 2 m/s, while peak ebb velocities range between 0.8 and 1.5 m/s during the spring-neap cycle. At location H2, flood velocities are relatively low for all tides (i.e., ~0.5 m/s) and ebb velocities exceed flood velocities by up to more than a factor two during spring tide (i.e., ebb velocities are up to ~1.2 m/s). At locations H3 and H4, at the southeastern side of the Hansweert sill (near the Walsoorden shoal), maximum flood velocities exceed maximum ebb velocities for all tides. It must, however, be stated that spring tides were not measured at location H3. Peak flood velocities at location H4 are up to 1.9 m/s for spring tide and 1.2 m/s for neap tide, while peak ebb velocities range between 0.6 and 1.2 m/s.

At locations H1 and H2, on the shallow plateau between the Ossenisse shoal and the Hansweert sill, additional velocity peaks are observed during higher high waters between May 7, 2016 and May 11, 2016. These additional velocity peaks can be attributed to circular flow patterns or eddies that develop over the Ossenisse shoal and the shallow plateau where the measurements were carried out. In particular, the flow direction during regular or lower tides have a flow direction that gradually shifts from flood direction (i.e., ~150° at locations H1 and H2) over westerly directions towards ebb direction (i.e., ~330° at locations H1 and H2). If additional eddy-induced velocity peaks during high water are present, the flow direction also shifts from flood direction to ebb direction (i.e., from ~150° to ~330°–360°), after which the flow direction rapidly changes to about 270°–300° and back to about 330°–360°.

An ensemble analysis was performed at location H1 for tides resulting in strong and weak cross-currents, using a threshold magnitude of the cross-current of 0.4 m/s, which corresponds with the mean value of the calculated cross-currents during the measurement campaign. Cross-currents are defined as the flow portion perpendicular to the mean flow direction. Zimmermann (1990) reports maximum cross-currents of 0.3 m/s for canals, without endangering safe navigation. Although the navigation channel in the Scheldt-estuary should not be seen as a canal, this value is comparable to the chosen threshold of 0.4 m/s.

It can be seen (Fig. 4) that strong cross-currents occur during stronger tides (i.e., tides with a large tidal range), resulting in larger water level gradients between the Hansweert and Walsoorden tidal stations (not shown) and also leading to higher flow velocities in the area of interest. The strongest cross-currents occur between the moment of high water and 60 min after high water, and can reach values up to 0.85 m/s. Over the total measurement campaign
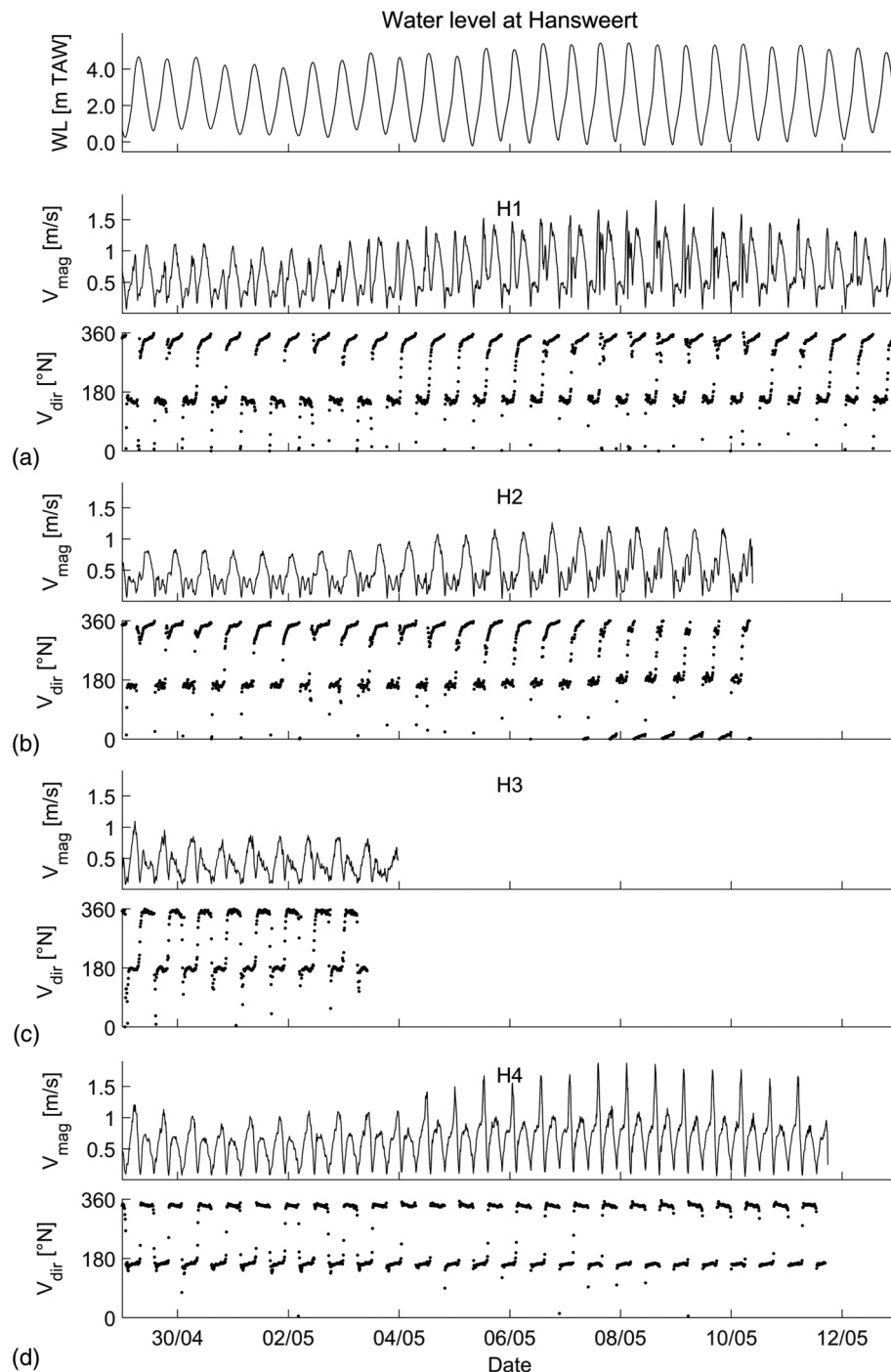
Fig. 3. Observed water levels at Hansweert and flow velocities and directions at locations: (a) H1; (b) H2; (c) H3; and (d) H4 during the 2016 measurement campaign.

(54 tides), the cross-currents were larger than 0.4 m/s during 25 tidal cycles (i.e., corresponding to 46% of the tides), larger than 0.6 m/s during 10 tidal cycles (19%), and larger than 0.8 m/s during 2 tidal cycles (4%).

Model Results

Water Levels

Table 2 gives an overview of the NeVla model performance for the representation of water levels along the estuary during the measurement period. The NeVla model represents the tidal propagation fairly well in the Western Scheldt, from where the model performance gradually decreases upstream. It should, however, be stated that especially high water levels in the study area are slightly overestimated (i.e., +0.08 m on average at the Hansweert tidal station). The high- and low-water phase errors are all smaller than the output interval of 10 min. After calibration by lowering bottom friction coefficients locally near the Ossenisse shoal and shallow plateau, the representation of water levels along the estuary remained similar. Besides, the presented model performance in Table 2 may deviate from the model performance that is presented
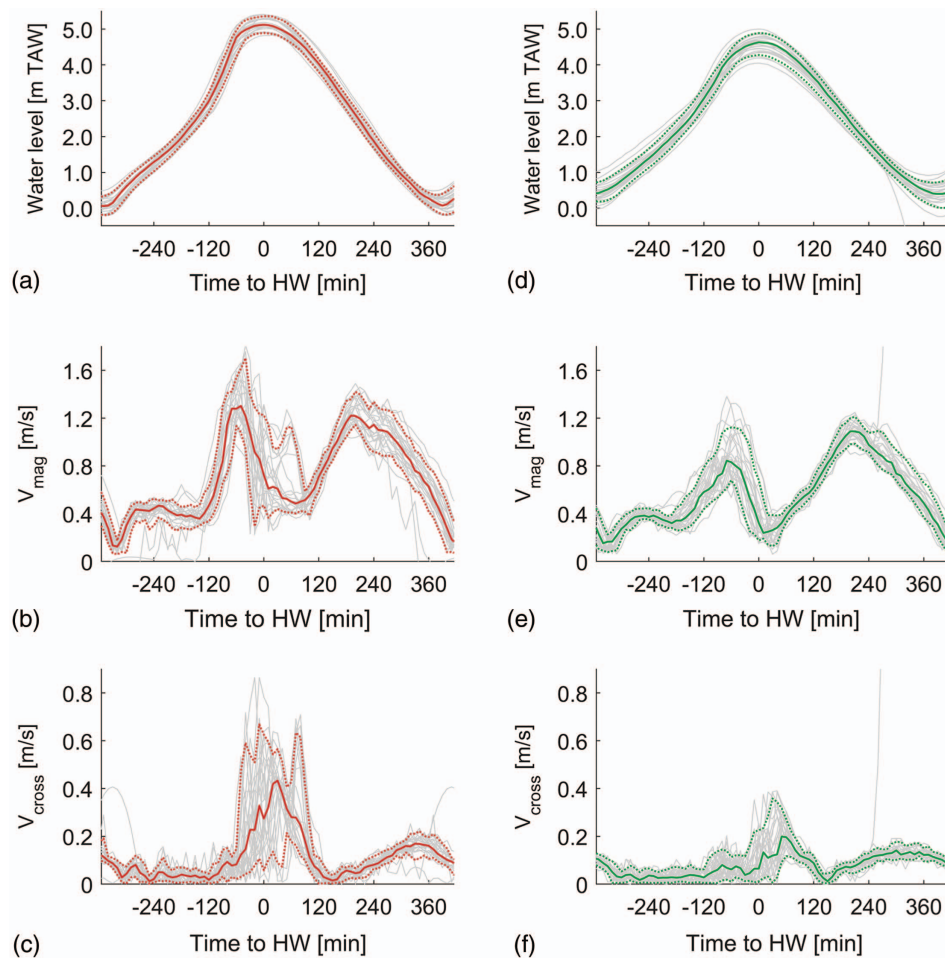
Fig. 4. (Color) Ensemble analysis of observed water levels at Hansweert for tides with (a) strong and (d) weak cross currents; (b, e) flow magnitude; and (c, f) cross current magnitude at location H1.

Table 2. Validation overview of the Delft3D NeVla (bold) and TELEMAC (italic) base runs based on observed water levels at tidal stations along the estuary, depicting the mean error (ME) and root-mean-squared error (RMSE) of the full time series as well as the ME and phase errors ($\Delta\varphi$) for the high and low waters

Location	Total series		High water		Low water	
	ME (m)	RMSE (m)	ME_{HW} (m)	$\Delta\varphi_{HW}$ (min)	ME_{LW} (m)	$\Delta\varphi_{LW}$ (min)
Cadzand	—	—	—	—	—	—
	+0.03	*0.13*	*0.0*	*+8.0*	*+0.01*	*−4.5*
Vlissingen	**+0.02**	**0.05**	**+0.01**	**0.0**	**+0.05**	**−2.5**
	+0.03	*0.14*	*0.0*	*+5.0*	*+0.03*	*−10.6*
Terneuzen	**+0.01**	**0.11**	**+0.04**	**−4.5**	**+0.04**	**−7.5**
	+0.02	*0.15*	*−0.01*	*+5.5*	*−0.02*	*−7.1*
Hansweert	**−0.01**	**0.09**	**+0.07**	**−3.0**	**−0.01**	**−5.8**
	−0.01	*0.18*	*+0.04*	*+2.7*	*−0.07*	*−10.8*
Walsoorden	**−0.01**	**0.09**	**+0.08**	**−4.7**	**−0.03**	**−4.7**
	−0.01	*0.19*	*+0.05*	*+1.9*	*−0.09*	*−10.6*
Bath	**+0.04**	**0.13**	**+0.11**	**−4.2**	**+0.04**	**−5.9**
	+0.03	*0.22*	*+0.11*	*+2.0*	*−0.08*	*−6.8*
Prosperpolder	**+0.04**	**0.14**	**+0.11**	**−5.8**	**+0.02**	**−7.0**
	+0.03	*0.23*	*+0.12*	*+1.1*	*−0.09*	*−6.0*
Liefkenshoek	**+0.03**	**0.15**	**+0.10**	**−2.3**	**+0.03**	**−5.9**
	+0.03	*0.24*	*+0.09*	*+1.4*	*−0.06*	*−5.2*
Antwerpen	**+0.04**	**0.18**	**+0.11**	**−2.3**	**+0.04**	**−8.8**
	+0.07	*0.26*	*+0.06*	*+4.2*	*+0.06*	*−1.0*

in previous Delft3D-NeVla (i.e., Maximova et al. 2014; Verheyen et al. 2013) or Scaldis (i.e., Smolders et al. 2016) validation reports as the simulation periods differ.

Where the Scaldis model is run using harmonic constituents at the seaward boundary, agreement with observed water levels throughout the estuary is expected to be better for the NeVla model than for the TELEMAC model (Table 2). In particular, RMSE-values are significantly higher for the TELEMAC model simulation. However, high- and low-water phases are of a similar accuracy as the Delft3D-NeVla model and the representation of high water levels is even better in the TELEMAC model.

The qualitative representation of complex flow patterns near the Hansweert sill and Ossenisse shoal is not expected to be influenced much by these small differences in tidal phase or amplitude, although it must be stated that Decrop et al. (2010) found that the presence of eddies and cross-currents in the study area is related to the magnitude of the high water level as well as local water level gradients (i.e., between Terneuzen, Hansweert, and Walsoorden). The model calibration efforts consisting of local bottom friction adaptations did not significantly change the estuary scale model performance regarding the vertical tide. In particular, water level errors only differ by up to 0.01 m, while high- or low-water level phase differences between the base and calibrated models are all lower than 1 min. As for the Delft3D model, the presented model performance of the TELEMAC model in Table 2 may again deviate
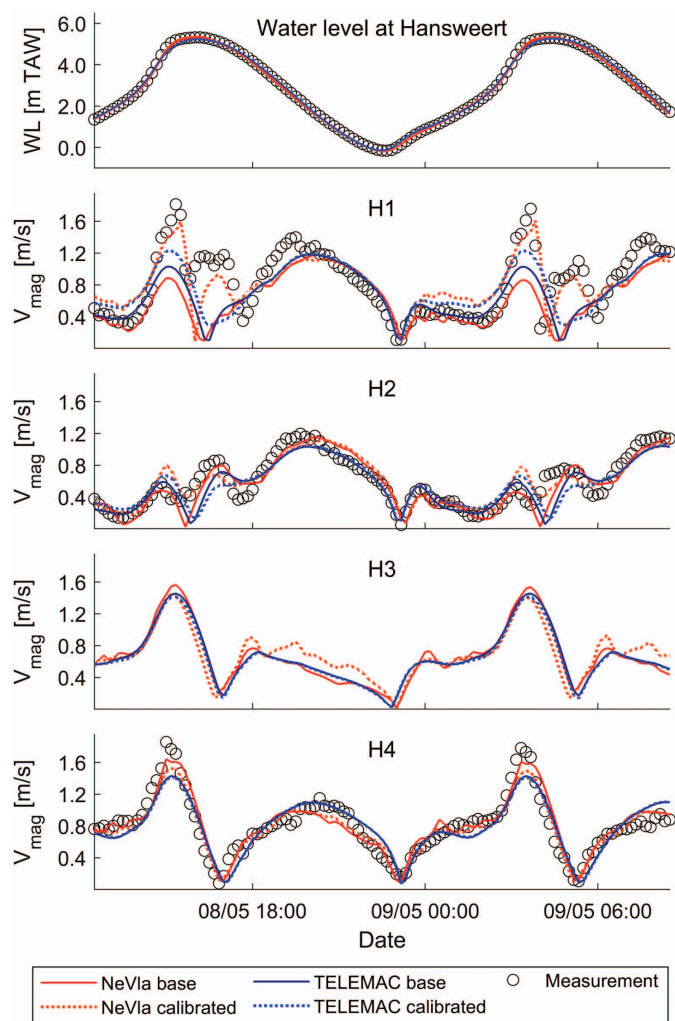
Fig. 5. (Color) Measured and modeled water levels at Hansweert and flow velocities at locations H1-H4 during spring tide.

Fig. 6. (Color) Measured and modelled water levels at Hansweert and flow velocities at locations H1-H4 during neap tide.
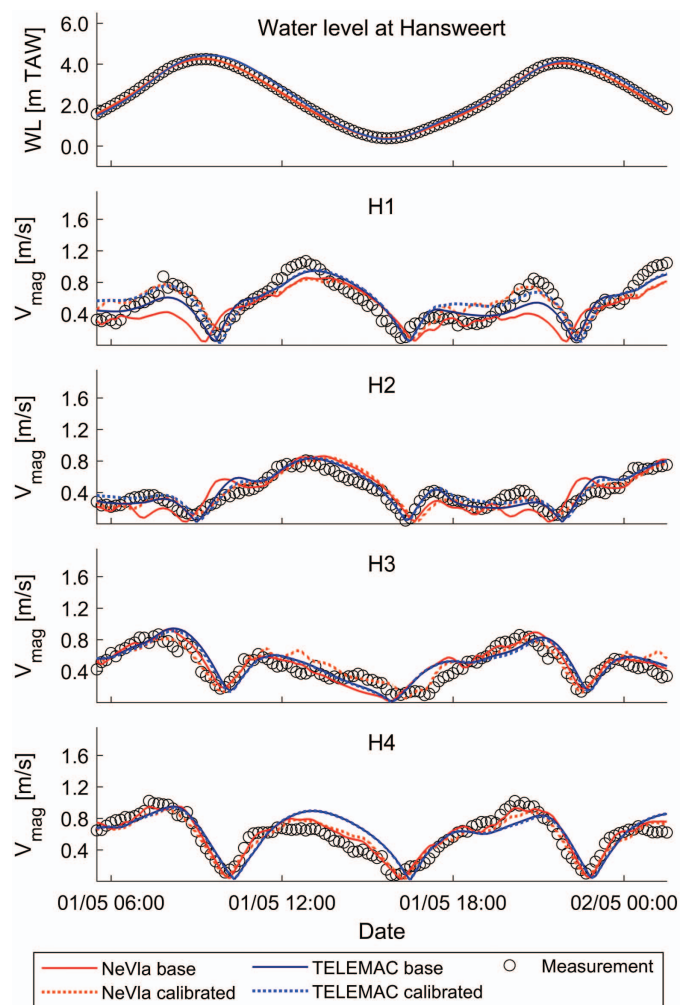
from the model performance presented in the Scaldis validation reports (Smolders et al. 2016; Vanlede et al. 2015) because the simulation periods and downstream boundaries are different.

Currents

Fig. 5 shows a comparison between the observed and modelled flow velocities at locations H1-H4 during a typical spring tide for the NeVla and TELEMAC models (i.e., base runs and calibrated runs), while Fig. 6 shows the results for a typical neap tide. The representation of the measured flow velocities during spring tide can only be assessed for locations H1, H2, and H4 because there is no data for location H3.

The measured flow velocities during neap tide are mostly well captured by both models at all four locations, although the TELEMAC base run and especially the NeVla base run underestimate the flood peak velocities at H1 by up to 0.5 m/s. Furthermore, both of the TELEMAC runs overestimate ebb velocities at location H4 during neap tide.

At location H4, situated at the opposite (i.e., southeastern) side of the Hansweert sill, the maximum spring tide velocities during flood are best represented by the NeVla models and somewhat more underestimated by the TELEMAC models. Contrastingly, the spring tide ebb velocities are well-captured by both TELEMAC models and underestimated by the NeVla models. Differences

between the base runs and calibrated runs are small at location H4, which can be explained by the fact that the bottom friction field in this area remains similar for all model runs [Fig. 2(b)].

At location H1, the strong ~2 m/s flood peak is only represented as such by the calibrated NeVla model, while the calibrated TELEMAC model and both base models still underestimate the maximum flood velocities at H1. The second velocity peak during high-water spring tide, associated with circular flows, is also best represented by the calibrated NeVla model. This additional velocity peak at H1 is not present in the other three model simulations. At location H2, however, the weaker second velocity peak during high water is to a certain extent represented in all four simulations. The spring flood peak itself at H2 is also well-represented in all simulations, although the calibrated models slightly overestimate the maximum flood velocities [i.e., up to +0.2 m/s for the calibrated NeVla model, which categorizes as "excellent" to "good" according to Sutherland et al. (2004)]. The ebb velocities at locations H1 and H2 on the shallow plateau are well captured by all models. Besides, differences in ebb velocities between the base runs and the calibrated models are remarkably small.

Over the same period as the measurement campaign (54 tides), the cross-currents in the calibrated NeVla model at location H1 were larger than 0.4 m/s during 39 tidal cycles (corresponding to 83% of the tides), larger than 0.6 m/s during 25 tidal cycles
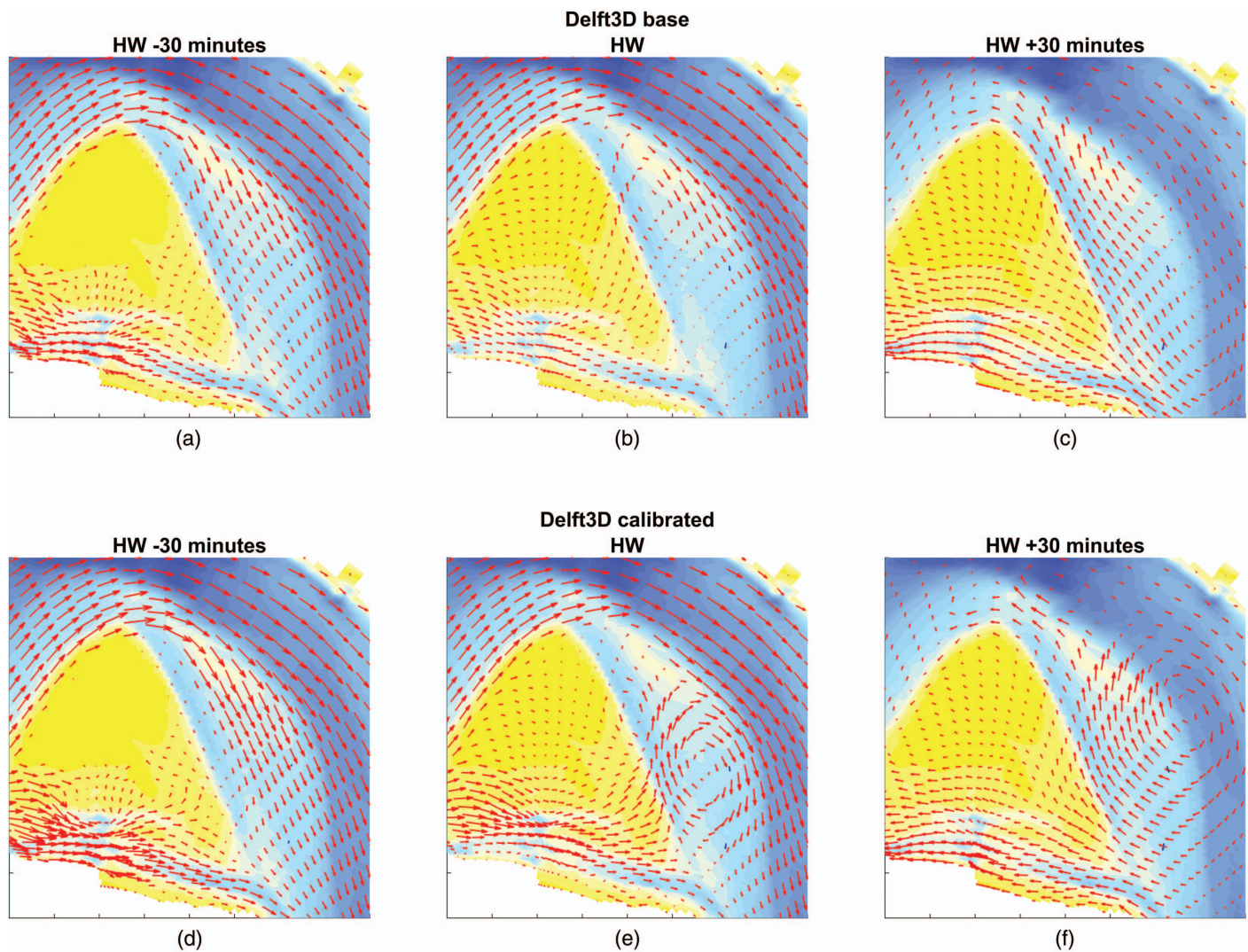
Fig. 7. (Color) Flow pattern in the study area: (a, d) 30 min before; (b, e) during; and (c, f) 30 min after high-water spring tide resulting from the Delft3D-NeVla (a–c) base and (d–f) calibrated model.

(46%), and were never larger than 0.8 m/s (0%). In comparison with the measurements, medium cross-currents (0.4 and 0.6 m/s) are modeled in almost twice the amount of tidal cycles as they were observed for. This implies that the calibrated NeVla model over-estimates the frequency of occurrence of eddy formation in the study area. This methodology could not be applied to the calibrated TELEMAC run because there are no distinct additional velocity peaks present at location H1 in this run.

In addition, Figs. 7 and 8 show the modelled velocity fields around spring-tide high water for the Delft3D-NeVla and TELEMAC models respectively. It is noted that the plotted velocity fields are more clear for the Delft3D model results, because this model has a structured grid, whereas the TELEMAC model consists of an un-structured grid.

The base runs of both models do not show strong circular flow patterns over the Ossenisse sandbar and shallow plateau around spring tide high water. In the base run of the NeVla model, how-ever, a small cross-directional flow develops at the northern part of the shallow plateau just before high water, but it doesn't develop into a large scale eddy. The TELEMAC base run has the opposite directed flows in the channel and on the shallow plateau existing next to each other, without any clear cross-directional flows be-tween them.

In contrast to the base runs, the calibrated NeVla and TELEMAC runs (i.e., with lowered bottom friction values on the shallow plateau) do produce circular flow patterns above the shallow plateau and adjacent channel. Based on the results of the calibrated NeVla model (Fig. 7), which captures the observed flow velocities and directions very well, the eddy forms around 30 min before high water above the shallow plateau between the sandbar and the sill of Hansweert. Near Hansweert, the flood current makes a turn of almost 180°, causing inertial effects that force the strong flood flow away from the eastern side of the sandbar, resulting in lower water levels at the plateau [Fig. 9(a)]. On the other hand, the flood flow simultaneously penetrates through the smaller connecting channel "Schaar van Ossenisse" south of the Ossenisse sandbar, resulting in higher water levels south of the plateau. The spatial water level variation shown in Fig. 9(a) shows a distinct water level depression of up to about 0.15 m over a distance of less than one kilometer between this connecting channel and the center of the depression. The water level depression on the plateau attracts water from this connecting channel in the south as well as from the navigation channel in the north. The local topo-bathymetry of the sandbar, which is lower at the south-eastern side, allows water to flow more easily from the south, over the south-eastern tip of the sandbar, to fill the depression. The corresponding strong currents flowing
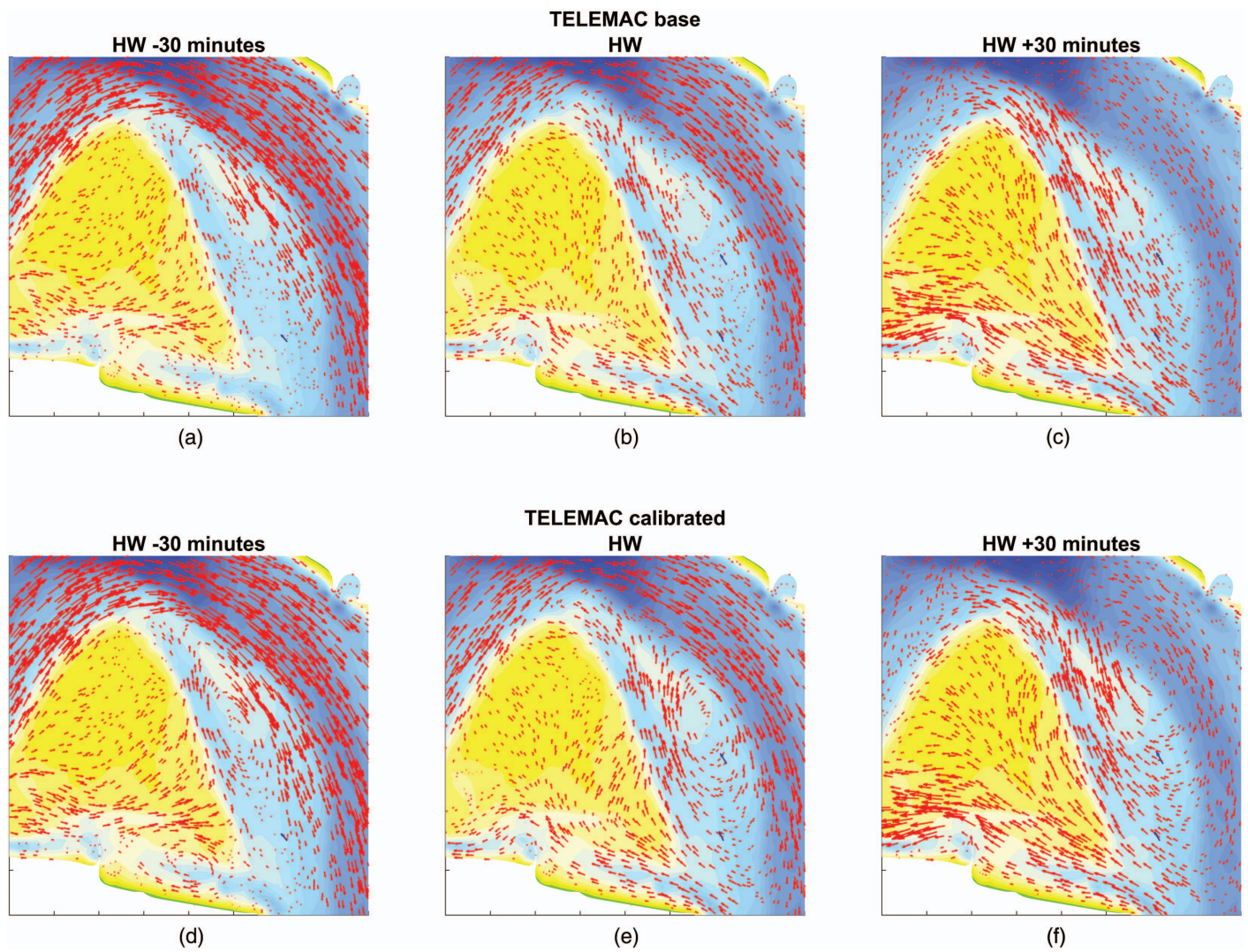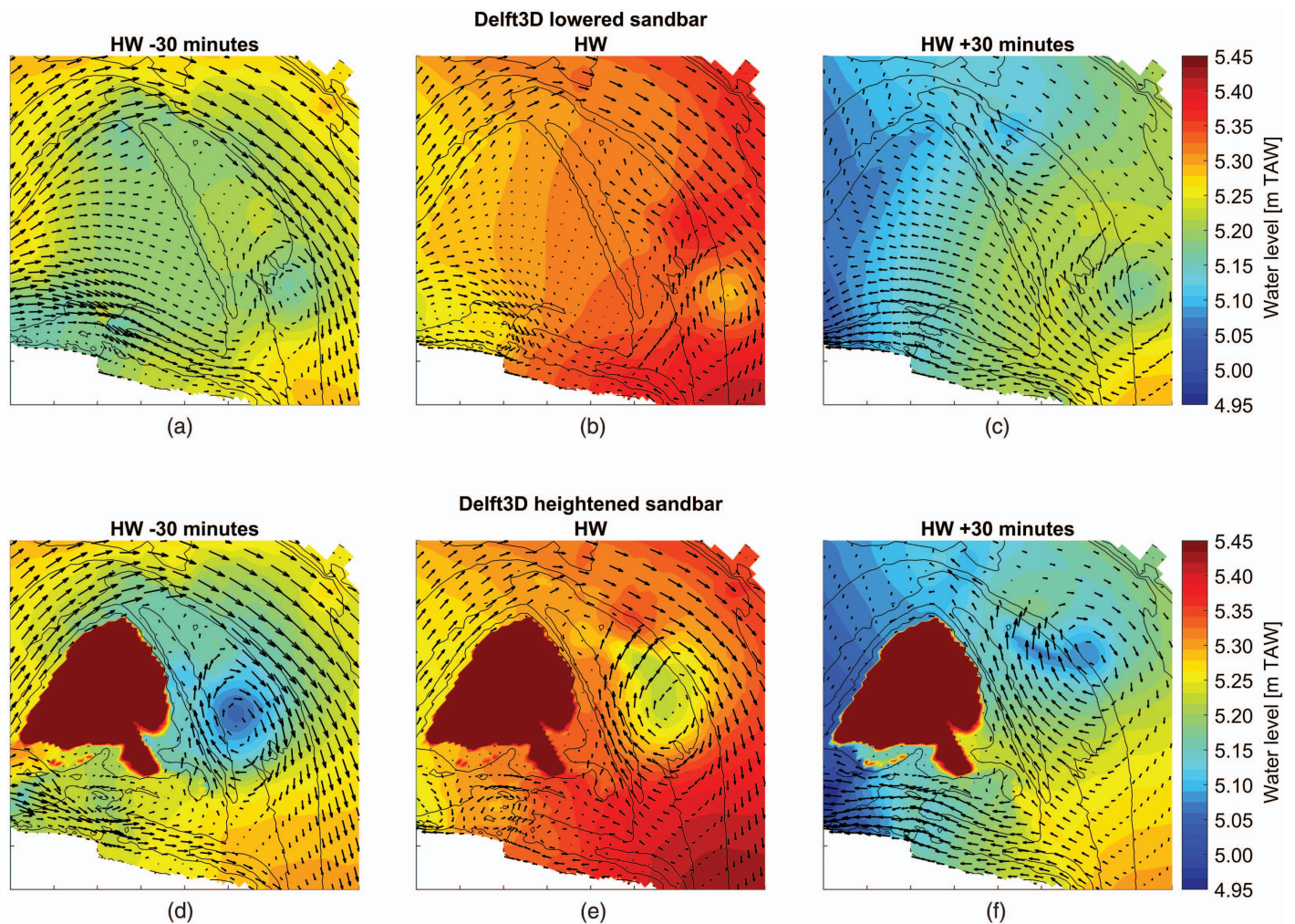
Fig. 8. (Color) Flow pattern in the study area: (a, d) 30 min before; (b, e) during; and (c, f) 30 min after high-water spring tide resulting from the TELEMAC (a–c) base and (d–f) calibrated model.
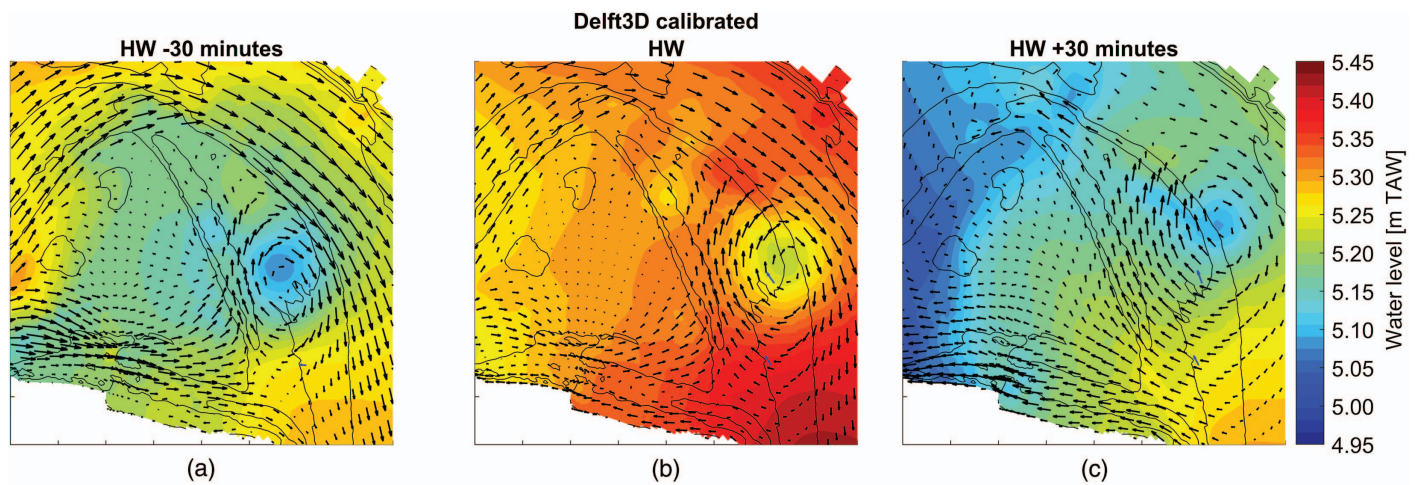
Fig. 9. (Color) Modeled water levels (m TAW) and velocities in the study area: (a) 30 min before; (b) during; and (c) 30 min after high-water spring tide resulting from the calibrated Delft3D-NeVla base model.

Fig. 10. (Color) Modeled water levels (m TAW) and velocities in the study area: (a, d) 30 min before; (b, e) during; and (c, f) 30 min after high-water spring tide resulting from the Delft3D-NeVla scenarios with a (a–c) lowered and (d–f) heightened Ossenisse sandbar.

towards the north, in combination with the strong flood currents in the navigation channel towards the south, then initiate the eddy as both flows start to curve around the center of the depression. Shortly after high water, the eddy has moved towards the channel where it increases in size, but decreases in strength and fades away shortly after. Nevertheless, eddy-induced cross-currents are simulated in the navigation channel with the calibrated NeVla model.

The calibrated TELEMAC model also produces a circular flow pattern, but the location and size of the eddy, as well as the flow speed and directions, correspond less good with the observed velocity vectors (Fig. 8). In particular, the cross-directional velocities (i.e., perpendicular to the ebb-flood-direction) are lower than the observed velocities and the large eddy itself is situated too far to the north on the shallow plateau. Eddy-induced cross-currents in the navigation channel are limited in the calibrated TELEMAC run as the eddy itself seems to be too weak to alter flow directions in the deep subtidal channel itself.

Model versus Measurements

Analysis of the driving mechanisms behind the cross-currents shows differences between the measurements and the calibrated NeVla model, both for high water levels in Hansweert and maximum flow velocities on the shallow plateau (Fig. 11). In both cases, the

model overestimates cross-currents. This also translates into a different occurrence frequency of the cross-currents during the measurement period (46% instead of 19% of the tidal cycles within the measurement period for which the modelled cross-current was larger than 0.6 m/s).

Scenarios

Both scenarios with altered elevation of the Ossenisse sandbar result in the formation of a large eddy at the eastern edge of the Ossenisse sandbar (Fig. 10). However, both the location of the center of the eddy and the cross-currents generated by the eddy are different. Due to the shift in the location of the center of the eddy, it is difficult to analyze cross-currents at one fixed point as was done for the model validation. Instead, it is opted to analyze the spatial flow patterns during the period of 30 min before to 30 min after high water.

In the scenario with the lowered sandbar, currents over the sandbar are stronger 30 min before high water, while the eddy is not as strong as in the reference run (i.e., the calibrated NeVla model run) at this time of the tidal cycle. At the moment of high water and 30 min after high water, the eddy remains weaker compared to the reference and the position of the center of the eddy is situated more to the south. The spatial water level differences of approximately 0.10 m are also smaller in this eddy. Besides, currents over the

sandbar at the start of the ebb phase (HW + 30′) are stronger in this scenario compared to the reference run.

In the scenario with the heightened sandbar, a large part of the sandbar remains dry during the simulated spring tide. Consequently, more water is forced around this dry part of the sandbar (i.e., through the small channel south of the Ossenisse shoal). At the three visualized moments of the tidal cycle (i.e., before, at, and after high water) a strong eddy is formed in this scenario, resulting in similar cross-currents as in the reference run. Both 30 min before and at high water, the center of the eddy is situated more to the west (closer to the eastern edge of the sandbar) compared to the reference, while 30 min after high water the center has moved to the north. The maximum water level depression in the eddy is slightly larger than in the calibrated NeVla reference run (i.e., up to ~0.17 m between the connecting channel and the center of the eddy).

Discussion

In order to reproduce the complex flow patterns near the sill of Hansweert, existing numerical models of the Scheldt estuary require specific calibration in which bottom roughness values are lowered locally on shallow and intertidal areas. A parametrization of bottom roughness based on sediment and bedform characteristics did not result in satisfactory results and therefore a pragmatic best-fit parametrization of bottom roughness was applied. This opens the discussion on the physical meaning of bottom roughness in the numerical models: when a physical based parametrization is not applicable due to spatial and temporal variation of hydrodynamics (e.g., water depth, flow direction) and sedimentology (e.g., grain size and bedforms), bottom roughness becomes purely a calibration parameter, not respecting the physical meaning of it. Another relevant aspect is the lack of numerical convergence of these models. This was not addressed in this paper, although other studies (Stark et al. forthcoming) show the influence of grid resolution on the results. Refinement of the numerical grid leads to differences in modeling results. However, all models are calibrated by changing both bed roughness and model diffusivity, resulting in a specific combination of these parameters for a certain grid resolution. This leads to a similar agreement (ME, RMSE) with the measurements.

After this calibration, both tested models (i.e., Delft3D-NeVla and TELEMAC) are able to represent the eddy formation above the shallow plateau in between the Ossenisse sandbar and the navigation channel. Besides, the local friction adaptations have a minimal impact on the overall model performance in terms of tidal propagation in the estuary. Because the models are only able to produce large-scale eddies in the study area if the bottom friction is significantly lowered on the shallow and intertidal areas (i.e., from $n = 0.025$ m$^{1/3}$ s^{-1} to $n = 0.015$ m$^{1/3}$ s^{-1}), this suggests that the shallow plateau and Ossenisse sandbar are actually smoother than areas elsewhere in the estuarine channel system. For the intertidal part, visual analysis of satellite images by Decrop et al. (2009) confirms this hypothesis. In particular, they identified a region where the sandbar consist of large mega ripples (i.e., mainly at the northern, western, and southern edges of the sandbar) and a region where the sandbar is much more flat and wet (i.e., situated at the center and eastern half of the Ossenisse sandbar). An analysis of the bedform characteristics based on recent multibeam echo soundings, show a large variation of the bedforms in the subtidal area around the Ossenisse sandbar, ranging from smaller dunes on the western and eastern edge of the sandbar (i.e., length ~10 m, height ~0.2 m) to larger dunes on the northern edge of the sandbar (i.e., length

~25 m, height ~1 m) (Plancke et al. 2018). In addition, suspended sediment samples that were obtained near the plateau during the measurement campaign presented by Vandebroek et al. (2017) reveal a substantial silt fraction at the plateau as 50%–90% of the suspended sediment samples. In contrast to the spatial variation in bedform characteristics, which is not clearly related with depth, the presence of cohesive sediments in the water column above the shallow plateau could support the hypothesis of a relatively smooth bottom in this area. Nevertheless, it cannot be excluded that the lower friction values are just a numerical solution to enhance tidal propagation over the tidal flat in the hydrodynamic models.

Large-scale eddies are formed in the occurrence of major differences in flow velocities. A large gyre can be found at groyne fields or at harbors perpendicular to rivers (Uijttewaal et al. 2001). These situations are characterized by a flowing water body that is in contact with an enclosed water body. The Ossenisse area has similarities, i.e., important tidal currents in the deeper channels and a shadow zone at the eastern edge of the Ossenisse shoal (primary driving mechanism), but also differs as water can flow from the channel located south of the shoal, which can be seen as a secondary driving mechanism for the formation of the large eddy.

In accordance with previous findings by Decrop et al. (2010), analysis of the driving factors behind cross-currents near the sill of Hansweert confirms the importance of the high water level in Hansweert for the occurrence of these cross-currents. For the present measurements, the predictive parameter for the occurrence of cross-currents presented in that previous study (i.e., cr) does however result in a weaker correlation (i.e., $R^2 = 0.60$) than the correlation with either the high water level in Hansweert (i.e., $R^2 = 0.78$) or the maximum flow velocity (which is related to the tidal range and thus high water level) at location H1 (i.e., $R^2 = 0.81$) as shown in Fig. 11. The change in correlation between the measured cross-currents and cr is possibly related to changes in (local) morphology, resulting in different contributions of driving forces behind the large eddies. In particular, the extent of the shallow plateau between the Ossenisse sandflat and the navigation channel increased since the study by Decrop et al. (2010). It should, however, be stated that the cr parameter does still give a strong correlation with the modeled cross-currents.

Model scenarios, in which the elevation of the Ossenisse sandbar is lowered or heightened, allow better insight into the driving processes behind the formation of the large eddy. In this study, the impact of elevation changes of the Ossenisse sandbar is assessed with two morphological scenarios. Changes in elevation of the Ossenisse sandbar significantly influence the formation of the large eddy (Fig. 10). If the sandbar is lowered, more water is able to flow over the sandbar towards the plateau, resulting in a smaller depression at the plateau and hence in a weaker eddy. Besides, the eddy is pushed more to the east due to the flood current over the sandbar. Conversely, when it is heightened, no water is able to flow over the sandbar, resulting in a slightly larger depression at the shallow plateau, because water from the southern connecting channel has to follow a longer route through the connecting channel before it is able to turn towards the depression. Because the ebb flow is not able to flow over the sandbar, the eddy is pushed further towards the north by the redirected ebb flow. The formation, size, and location of the eddy are thus affected by the elevation morphology of the Ossenisse sandbar. Other morphological features that are thought of to have an influence on the eddy formation based on the model scenarios are the shallow plateau (i.e., as the eddy is actually initiated here) and the "Schaar van Ossenisse" south of the sandbar (i.e., as the flood flow through this connecting channel appears to be crucial for the initiation of the eddy).
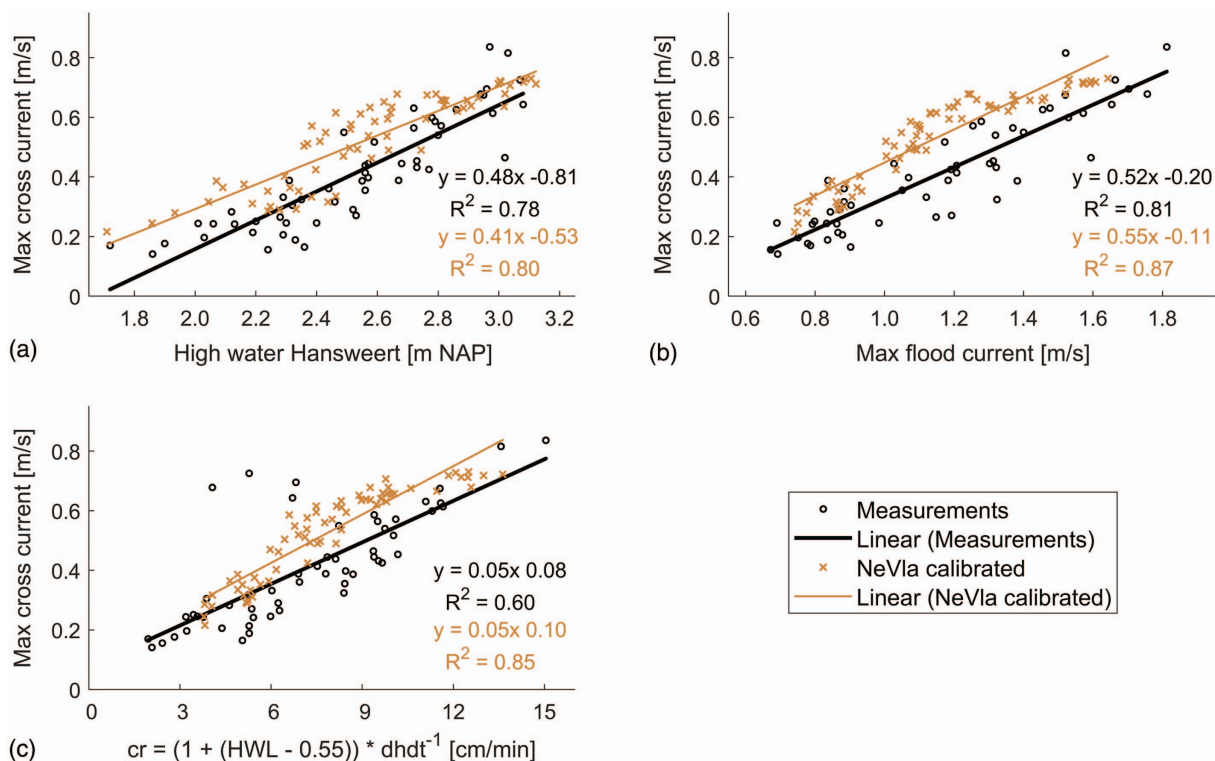
Fig. 11. (Color) Relations between (a) high-water level at Hansweert; (b) maximum flood velocities at H1; and (c) the *cr* parameter developed by Decrop et al. (2010) at Hansweert and maximum cross-currents at location H1 from measurements (black circles) and the calibrated NeVla model (orange cross marks).

Conclusions

This study presents the analysis of flow measurements conducted near Hansweert in the Scheldt estuary in combination with the validation of two hydrodynamic models of the Scheldt estuary. This location is situated near the intensively dredged Hansweert sill and covers an area in which cross-currents occur that cause an important challenge for shipping. The calibrated Delft3D-NeVla model gives the best model performance regarding the reproduction of the measured flow velocities. It successfully captures the strong velocity peaks associated with the flood flow over the Ossenisse sandbar and the flood peaks associated with eddy-induced currents on the shallow plateau, which are both underestimated by the TELEMAC model. Nevertheless, the frequency of occurrence of the eddy formation during higher high waters is overestimated by the Delft3D-NeVla model. This implies that if the model results are used to set up criteria for the prediction of hazardous cross-currents as done previously by Decrop et al. (2010), the present-day risk for shipping traffic will be slightly overestimated. From the data analysis it was found that these cross-currents occur mainly at strong spring tides, which have higher high water levels and stronger flood currents. Numerical model scenarios additionally show that the elevation and morphology of the sandbar have a large influence on the development of eddies in the study area.

Overall, the results of this validation study may assist estuarine managers as adequate model predictions of tidal hydrodynamics are of importance for navigation purposes (e.g., Decrop et al. 2009, 2010), but also for safety against flooding (e.g., Meire et al. 2014; Smolders et al. 2015) and sediment management (e.g., Bolle et al. 2010; Plancke et al. 2015). Because the complex flow fields are represented sufficiently in the models, they can be implemented in the ship simulator for river pilots training. This allows pilots to gain experience on how to deal with and improve their awareness of these complex flow fields, which will result in safer navigation in the field.

Acknowledgments

References

Adams, R., D. Depreiter, G. Van Holland, M. De Beuckelaer-Dossche, and G. Van Ryckegem. 2016. "Integrated plan of the upper sea Scheldt: Towards a sustainable future." In *Book of abstracts: ECSA Local Meeting 2016. Estuarine Restoration: From theory to practice and back*, edited by P. Meire, 72. Antwerp, Belgium: Univ. of Antwerp.

Baeyens, W., B. van Eck, C. Lambert, R. Wollast, and L. Goeyens. 1998. "General description of the Scheldt estuary." In *Trace metals in the Westerschelde Estuary: A case-study of a polluted, partially anoxic estuary*, 1–14. Dordrecht, Netherlands: Springer.

Bolle, A., Z. Bing Wang, C. Amos, and J. De Ronde. 2010. "The influence of changes in tidal asymmetry on residual sediment transport in the Western Scheldt." *Cont. Shelf Res.* 30 (8): 871–882. https://doi.org/10.1016/j.csr.2010.03.001.

Chow, V. Te 1959. *Open-channel hydraulics*. New York: McGraw-Hill.

Cornet, E., and F. Mostaert. 2010. *Hydrologisch jaarboek 2009: HIC meetstations*. WL Rapporten. Antwerpen, Belgium: Waterbouwkundig Laboratorium.

Cox, T., T. Maris, P. De Vleeschauwer, T. De Mulder, K. Soetaert, and P. Meire. 2006. "Flood control areas as an opportunity to restore estuarine habitat." *Ecol. Eng.* 28 (1): 55–63. https://doi.org/10.1016/j.ecoleng.2006.04.001.

Dauwe, W., P. Meire, T. Maris, P. Peeters, L. Coen, M. Deschamps, J. Rutten, and S. Temmerman. 2014. "The recent 'Saint Nicholas' storm surge in the Scheldt estuary: The Sigma plan proves its efficiency!" *ECSA Bull.* 62: 19–23.

Decrop, B., B. De Clercq, J. Vanlede, and M. Sas. 2010. "Eddy-induced cross currents in the Westerschelde estuary: Numerical simulation, physical driving mechanisms and navigation assistance." *Bull. Perm. Int. Assoc. Navig. Congr.* 138: 29–44.

Decrop, B., B. De Clercq, J. Vanlede, G. Van Holland, S. Ides, Y. Plancke, T. De Mulder, and F. Mostaert. 2009. *Dwarsstromingen Ossenisse-Zuidergat—Rapport numeriek modelonderzoek. WL Rapporten 753_07. Waterbouwkundig Laboratorium en IMDC rapport nr. I/RA/11313/09.009/BDC*. Antwerp, Belgium: Flanders Hydraulics Research.

Deltares. 2016. *Delft3D-FLOW, user manual*. Delft, Netherlands: Deltares.

de Vet, P. L. M., B. C. van Prooijen, and Z. B. Wang. 2017. "The differences in morphological development between the intertidal flats of the Eastern and Western Scheldt." *Geomorphology* 281 (Mar): 31–42. https://doi.org/10.1016/j.geomorph.2016.12.031.

De Vriend, H. J., Z. B. Wang, T. Ysebaert, P. M. J. Herman, and P. Ding. 2011. "Eco-morphological problems in the Yangtze Estuary and the Western Scheldt." *Wetlands* 31 (6): 1033–1042. https://doi.org/10.1007/s13157-011-0239-7.

De Wit, K., Y. Meersschaut, and M. Sas. 2007. "Third enlargement program of the river Scheldt." In *Proc., Papers and Presentations of the World Dredging Conf. (WODCON XVIII)*, 667–682. Orlando, FL.

EDF R&D (Electricité de France Research & Development). 2017. *Telemac3D user manual*. Chatou, France: EDF R&D.

Elias, E. P. L., A. J. F. van der Spek, and M. Lazar. 2017. "The 'Voordelta', the contiguous ebb-tidal deltas in the SW Netherlands: Large-scale morphological changes and sediment budget 1965–2013; impacts of large-scale engineering." *Neth. J. Geosci.* 96 (3): 233–259. https://doi.org/10.1017/njg.2016.37.

Eloot, K., and J. Verwilligen. 2010. "Synergy between theory and practice for ultra large container ships." In *Proc., 32nd PIANC Congress, 125th Anniversary PIANC—Setting the Course, Liverpool, UK, Liverpool Arena and Convention Centre, 10–14 May 2010: PIANC MMX papers, PIANC. UK section*, 188. Liverpool, UK: Liverpool Arena and Convention Centre.

French, P. W. 2006. "Managed realignment—The developing story of a comparatively new approach to soft engineering." *Estuarine Coastal Shelf Sci.* 67 (3): 409–423. https://doi.org/10.1016/j.ecss.2005.11.035.

Gerritsen, H., E. D. de Goede, F. W. Platzek, M. Genseberger, J. A. T. M. van Kester, and R. E. Uittenbogaard. 2007. *Validation document Delft3D-FLOW*. Delft, Netherlands: Deltares.

Hervouet, J.-M. 2007. *Hydrodynamics of free surface flows: Modelling with the finite element method*. Chichester, UK: Wiley.

Ides, S., and Y. Plancke. 2008. *Determinatieonderzoek plaatrandstortingen: deelrapport 2. Numerieke modellering*. WL Rapporten. Antwerpen, Belgium: Waterbouwkundig Laboratorium.

Ides, S. J., Y. M. G. Plancke, and G. R. Vos. 2010. "Validation of a 2D hydrodynamic model within a study to propose the optimal disposal strategy in the Western Scheldt." In *Proc., SIMHYDRO 2010: modèles hydrauliques et incertitudes, Nice, 2-4 juin 2010 [CD-ROM]*, 1–9. Paris: Société Hydrotechnique de France.

Maximova, T., S. Ides, J. Vanlede, T. De Mulder, and F. Mostaert. 2009. *Verbetering 2D randvoorwaardenmodel: deelrapport 3. Kalibratie bovenlopen*. WL Rapporten. Antwerpen, Belgium: Waterbouwkundig Laboratorium.

Maximova, T., J. Vanlede, B. De Maerschalck, T. van Oyen, T. Verwaest, and F. Mostaert. 2014. *Verbetering morfologisch instrumentarium: subreport 2. Modellentrein DCSMv5–ZUNOv3: validatie modelrun 2014*. WL Rapporten. Antwerpen, Belgium: Waterbouwkundig Laboratorium.

Meire, P., T. Ysebaert, S. Van Damme, E. Van Den Bergh, T. Maris, and E. Struyf. 2005. "The Scheldt estuary: A description of a changing ecosystem." *Hydrobiologia* 540 (1–3): 1–11. https://doi.org/10.1007/s10750-005-0896-8.

Mitchell, S. B. 2013. "Turbidity maxima in four macrotidal estuaries." *Ocean Coastal Manage.* 79 (2013): 62–69. https://doi.org/10.1016/j.ocecoaman.2012.05.030.

Peters, J. J., J. A. Cunge, and Y. M. G. Plancke. 2006. "Role of practinioners and hydroinformatics in the decision-making process for morphological management of an estuary." In *Proc., 7th Int. Conf. on Hydroinformatics*, edited by P. Gourbesville, et al., 1–8. Chennai, India: Research Publishing.

Plancke, Y., D. Meire, and F. Mostaert. 2018. *Agenda voor de toekomst—Morfologie Mesoschaal: deelrapport 14. Bodemtransport nabij de Platen van Ossenisse op basis van een analyse van bodemvormen*. WL Rapporten. Antwerpen, Belgium: Waterbouwkundig Laboratorium.

Plancke, Y., E. Vanlierde, and E. Taverniers. 2012. "Monitoring of physical parameters within the scope of the Dutch-Flemish integrated monitoring program." In *Proc., Hydraulic Measurements and Experimental Methods 2012 Conf.*, edited by F. Mostaert, 1–6. Reston, VA: ASCE.

Plancke, Y., G. R. Vos, and M. Schrijver. 2015. "New disposal strategy in the Schelde-estuary: Using dredged sediment to create benefits for nature." In *Proc., E-Proceedings of the 36th IAHR World Congress*, 1–7. The Hague, Netherlands.

Rijkswaterstaat Directie Zeeland and Ministry of the Flemish Government. 2001. *Long term vision schelde-estuary*. Brussels, Belgium: Flemish Government.

Rupp-Armstrong, S., and R. J. Nicholls. 2007. "Coastal and estuarine retreat: A comparison of the application of managed realignment in England and Germany." *J. Coastal Res.* 236 (6): 1418–1430. https://doi.org/10.2112/04-0426.1.

Smolders, S., T. Maximova, J. Vanlede, Y. Plancke, T. Verwaest, and F. Mostaert. 2016. *Integraal plan Bovenzeeschelde: Subreport 1. SCALDIS: A 3D Hydrodynamic model for the Scheldt Estuary*. WL Rapporten. Antwerpen, Belgium: Waterbouwkundig Laboratorium.

Smolders, S., Y. Plancke, S. Ides, P. Meire, and S. Temmerman. 2015. "Role of intertidal wetlands for tidal and storm tide attenuation along a confined estuary: A model study." *Nat. Hazards Earth Syst. Sci.* 15 (7): 1659–1675. https://doi.org/10.5194/nhess-15-1659-2015.

Stark, J., B. De Maerschalck, Y. Plancke, and F. Mostaert. Forthcoming. *AvdT—Sedimenttransport op verschillende tijdschalen: Deelrapport 3—Modellering van hydro- en morfodynamische processen in de Westerschelde met Telemac: Scenario's in het kader van gevoeligheidsanalyse numeriek model*. Antwerp, Belgium: Waterbouwkundig Laboratorium.

Stark, J., P. Meire, and S. Temmerman. 2017a. "Changing tidal hydrodynamics during different stages of eco- geomorphological development of a tidal marsh: A numerical modeling study." *Estuarine Coastal Shelf Sci.* 188 (Mar): 56–68. https://doi.org/10.1016/j.ecss.2017.02.014.

Stark, J., S. Smolders, P. Meire, and S. Temmerman. 2017b. "Impact of intertidal area characteristics on estuarine tidal hydrodynamics: A modelling study for the Scheldt Estuary." *Estuarine Coastal Shelf Sci.* 198 (Part A): 138–155. https://doi.org/10.1016/j.ecss.2017.09.004.

Strickler, A. 1923. *Beiträge zur Frage der Geschwindigheitsformel und der Rauhegkeitszahlen für Ströme, Kanäle und geschlossene Leitungen*. Bern, Switzerland: Mitteilungen des Amtes für Wasserwirtschaft.

Sutherland, J., D. J. R. Walstra, T. J. Chesher, L. C. van Rijn, and H. N. Southgate. 2004. "Evaluation of coastal area modelling systems at an estuary mouth." *Coastal Eng.* 51 (2): 119–142. https://doi.org/10.1016/j.coastaleng.2003.12.003.

Temmerman, S., and M. L. Kirwan. 2015. "Building land with a rising sea." *Science* 349 (6248): 588–589. https://doi.org/10.1126/science.aac8312.

Townend, I., and J. Pethick. 2002. "Estuarine flooding and managed retreat." *Philos. Trans. Royal Soc. Series A: Math. Phys. Eng. Sci.* 360 (1796): 1477–1495. https://doi.org/10.1098/rsta.2002.1011.

Uijttewaal, W. S. J., D. Lehmann, and A. Van Mazijk. 2001. "Exchange processes between a river and its Groyne fields: Model experiments." *J. Hydraul. Eng.* 127 (11): 928–936. https://doi.org/10.1061/(ASCE)0733-9429(2001)127:11(928).

Vandebroek, E., S. Claeys, Y. Plancke, T. Verwaest, and F. Mostaert. 2017. "Agenda for the future—Mesoscale hydro- and sediment dynamics in the Schelde estuary: Sub report 10. Factual data report for measurements at Drempel van Hansweert in April/May 2016." . FHR Rep. Antwerp, Belgium: Antea Group.

van der Wal, D., R. M. Forster, F. Rossi, H. Hummel, T. Ysebaert, F. Roose, and P. M. J. Herman. 2011. "Ecological evaluation of an experimental beneficial use scheme for dredged sediment disposal in shallow tidal waters." *Mar. Pollut. Bull.* 62 (1): 99–108. https://doi.org/10.1016/j.marpolbul.2010.09.005.

van der Wal, D., G. I. Lambert, T. Ysebaert, Y. Plancke, and P. M. J. Herman. 2017. "Hydrodynamic conditioning of diversity and functional traits in subtidal estuarine macrozoobenthic communities." *Estuarine Coastal Shelf Sci.* 197 (Oct): 80–92. https://doi.org/10.1016/j.ecss.2017.08.012.

Vanlede, J., B. De Clercq, B. Decrop, S. Ides, G. van Holland, T. De Mulder, and F. Mostaert. 2009. *Verbetering randvoorwaardenmodel: deelrapport 2. Afregelen van het 2D Scheldemodel.* WL Rapporten. Antwerpen, Belgium: Waterbouwkundig Laboratorium/IMDC.

Vanlede, J., S. Smolders, T. Maximova, and M. J. Teles. 2015. "The unstructured Scaldis model: A new 3D high resolution model for hydrodynamics and sediment transport in the tidal Scheldt." In *Proc., Scheldt Estuary: Physics and Integrated Management—Special Session on of the 36th IAHR World Congress*, 11. The Hague, Netherlands.

van Maren, B., and T. van Kessel. 2016. "Long-Term effects of maintenance dredging on turbidity." *Terra et Aqua* 145: 5–14.

van Rijn, L. C. 1984. "Sediment transport, Part III: Bed forms and Alluvial Roughness." *J. Hydraul. Eng.* 110 (12): 1733–1754. https://doi.org/10.1061/(ASCE)0733-9429(1984)110:12(1733).

Verheyen, B., J. Vanlede, B. Decrop, T. Verwaest, and F. Mostaert. 2013. *Verbetering randvoorwaardenmodel: deelrapport 5. Actualisatie van het 3D Scheldemodel.* WL Rapporten. Antwerpen, Belgium: Flanders Hydraulics Research.

Vos, G., K. Wouters, J. Deleu, D. Meire, Y. Plancke, T. Verwaest, and F. Mostaert. 2017. *Agenda voor de toekomst—Stroming en sedimenttransport op de mesoschaal in het Schelde-estuarium: deelrapport 1. Data-analyse sedimentdynamica ter hoogte van drempels.* WL Rapporten. Antwerpen, Belgium: Antea Group.

Wang, Z., C. Jeuken, and H. De Vriend. 1999. *Tidal asymmetry and residual sediment transport in estuaries. A literature study and applications to the Western Scheldt.* Z2749. Delft, Netherlands: WL Delft Hydraulics.

Winterwerp, J. C., Z. Bing, W. Alexander, G. Van Holland, and F. Kosters. 2013. "Man-induced regime shifts in small estuaries—II : A comparison of rivers." *Ocean Dyn.* 63 (11–12): 1293–1306. https://doi.org/10.1007/s10236-013-0663-8.

Zimmermann, C. 1990. "Zur frage zulässiger Querströmungen an Bundeswasserstrassen." *Mitteilungsblatt der Bundesanstalt für Wasserbau* 67 (67): 175–206.